Bottom water oxygenation changes in the Southwestern Indian Ocean as an indicator for enhanced respired carbon storage since the last glacial inception

Helen Eri Amsler[1,2], Lena M. Thöle[1,2,3], Ingrid Stimac[4], Walter Geibert[4], Minoru Ikehara[5], Gerhard Kuhn[4, 5] Oliver Esper[4], Samuel L. Jaccard[1,2]*

[1]Institute of Geological Sciences, University of Bern, Switzerland
[2]Oeschger Centre for Climate Change Research, University of Bern, Switzerland
[3]Department of Earth Sciences, Utrecht University, the Netherlands
[4]Alfred-Wegener-Institut Helmholtz-Zentrum für Polar- und Meeresforschung, Bremerhaven, Germany
10 [5]Center for Advanced Marine Core Research, Kochi University, Japan
* present affiliation: Institute of Earth Sciences, University of Lausanne, Switzerland

Correspondence to: H. Eri Amsler (helen-eri.amsler@geo.unibe.ch); Samuel Jaccard (samuel.jaccard@unil.ch)

Abstract.

We present downcore records of redox-sensitive authigenic uranium (U) and manganese (Mn) concentrations based on five

15 marine sediment cores spanning a meridional transect encompassing the Subantarctic and the Antarctic zones in the Southwest Indian Ocean covering the last glacial cycle. These records signal lower bottom water oxygenation during glacial climate intervals and generally higher oxygenation during warm periods, consistent with climate-related changes in deep ocean remineralised carbon storage. Regional changes in the export of siliceous phytoplankton to the deep-sea may have entailed a secondary influence on oxygen levels at the water-sediment interface, especially in the Subantarctic Zone. The

20 rapid reoxygenation during the deglaciation is in line with increased ventilation and enhanced upwelling after the Last Glacial Maximum (LGM), which, in combination, conspired to transfer previously sequestered remineralised carbon to the surface ocean and the atmosphere, contributing to propel the Earth's climate out of the last ice age. These records highlight the yet insufficiently documented role the southern Indian Ocean played in the air-sea partitioning of CO_2 on glacial-interglacial timescales.

25 **1 Introduction**

On glacial-interglacial timescales, the global ocean plays a dominant role in regulating changes in the exogenic carbon cycle (e.g. Sigman and Boyle, 2000). Indeed, the deep ocean has a sufficiently voluminous and dynamic carbon reservoir to modulate the air-sea partitioning of CO_2, and by inference, climate. In particular, the Southern Ocean acts as a major conduit connecting the vast ocean interior and the atmosphere, as deep CO_2-rich water masses outcrop along tilted density surfaces

30 (isopycnals) promoting exchange with the atmosphere (Marshall and Speer, 2012; Talley, 2013).

Accordingly, a number of distinct, often synergistic mechanisms, focusing on changes in Southern Ocean circulation, nutrient biogeochemistry and sea-ice dynamics have been proposed to have contributed to lower atmospheric CO_2 during past ice ages (e.g. Adkins, 2013; Ferrari et al., 2014; Hain et al., 2010; Sigman et al., 2010; Sigman et al., 2020). However, the mechanisms accounting for the generally reduced glacial atmospheric CO_2 inventory are still debated and not yet fully

35   resolved. Radiocarbon (^{14}C) data suggest that the deep (>1000–1500 m) ocean was generally more poorly ventilated during the last ice age (Sarnthein et al., 2013; Skinner et al., 2017) (although a portion of this signal could be related to decreased air-sea gas exchange (Galbraith et al., 2015)). The formation of saltier (less buoyant) bottom waters around Antarctica due to more dynamic sea-ice cycling would have strengthened the stratification and isolation of deeper waters during the Last Glacial Maximum (LGM) (Adkins, 2013; Adkins et al., 2002; Bouttes et al., 2010; Ferrari et al., 2014; Stein et al., 2020).

40   Furthermore, a northward shift of the upwelling region might have led to the exposure of shallower waters, resulting in reduced outgassing and enhanced carbon sequestration in the ocean interior (Sigman and Boyle, 2000; Toggweiler, 1999; Toggweiler et al., 2006; Watson et al., 2015).

In addition to these physical mechanisms affecting ocean circulation, changes in marine biology and nutrient biogeochemistry also contributed to sequester carbon away from the atmosphere (Francois et al., 1997; Galbraith and

45   Jaccard, 2015; Sigman and Boyle, 2000; Sigman et al., 2010; Sigman et al., 2020). A generally more efficient biological carbon pump during glacial periods, sustained by increased Fe-bearing dust supply and/or generally more complete nutrient utilization would have contributed to curb CO_2 outgassing from the Southern Ocean (e.g. Ai et al., 2020; Galbraith and Skinner, 2020; Gottschalk et al., 2016; Jaccard et al., 2013; Kohfeld et al., 2005; Kumar et al., 1995; Martínez-García et al., 2014; Sigman et al., 2010; Studer et al., 2015).

50   At the onset of the last glacial termination (TERM I), approximately 17.5 ka ago, Southern Ocean ventilation resumed as the Earth emerged from the last ice age, and previously sequestered, radiocarbon-depleted CO_2 was released to the atmosphere (e.g. Basak et al., 2018; Bauska et al., 2016; Burke and Robinson, 2012; Gottschalk et al., 2016; Gottschalk et al., 2020b; Jaccard et al., 2016; Rae et al., 2018; Skinner et al., 2010). Coupled with enhanced upwelling, nutrient- and CO_2-rich subsurface waters were transported to the sunlit surface ocean, supporting high levels of biological production south of the

55   Polar Front (e.g. Anderson et al., 2009; Frank et al., 2000; Jaccard et al., 2013; Kohfeld et al., 2005; Thöle et al., 2019). At the same time, Fe-bearing dust supply started to dwindle, causing biogenic export production to decline in the Subantarctic Zone (Anderson et al., 2014; Jaccard et al., 2016, 2013; Martínez-García et al., 2014; Thöle et al., 2019), further decreasing marine carbon storage.

Reconstructing past changes in bottom water oxygenation has the potential to further document some of these processes.

60   Indeed, variations in the storage of respiratory carbon are accompanied by large changes in dissolved oxygen concentration associated with organic matter remineralization (e.g. Anderson et al., 2019; Gottschalk et al., 2016; Gottschalk et al., 2020b; Hoogakker et al., 2015; Jaccard et al., 2016; Jacobel et al., 2017). The temporal evolution of bottom water oxygenation can thus be reconstructed qualitatively using the distribution of redox-sensitive metals in the marine sedimentary record (e.g. Calvert and Pedersen, 1996; Francois et al., 1997; Frank et al., 2000; Nameroff et al., 2002). Here we focus on authigenic

65   uranium (U) and manganese (Mn), which are both sensitive to dissolved oxygen concentrations typically encountered in open ocean conditions. The analyses were carried out on a set of five marine sediment cores spanning a meridional transect in the yet underrepresented Indian sector of the Southern Ocean. Combining these observations with preserved opal flux reconstructions allows for deciphering the different processes affecting bottom water oxygenation and inferring their relative contributions in sequestering CO_2 in the ocean interior.

70   **2 Study site, materials and methods**

2.1 Core locations and material

This study was carried out on five marine sediment cores, retrieved along a meridional transect including Del Caño Rise and Conrad Rise and reaching as far south as Enderby Abyssal Plain (Figure 2.1). Cores DCR-1PC (46°01.34'S, 44°15.24'E, 2632 mbsl) and COR-1bPC (54°16.04'S, 39°45.98'E, 2828 mbsl) were collected during expedition KH-10-7 on R/V
75   *Hakuho-maru* in 2010–2011. The sediment cores were retrieved from the southern flank of Del Caño Rise (DCR-1PC) and Conrad Rise (COR-1bPC), respectively. Cores PS2609-1 (51°29.9'S, 41°35.8'E, 3113 mbsl), PS2606-6 (53°13.9'S, 40°48.1'E, 2545 mbsl) and PS2603-3 (58°59.2'S, 37°37.7'E, 5289 mbsl) were retrieved during ANT-XI/4 expedition on R/V *Polarstern* in 1994. Cores PS2609-1 and PS2606-6 were retrieved from Conrad Rise as well, the former one on its northern flank and the latter on the rise itself. Core PS2603-3 is located furthest to the south in the Enderby Abyssal Plain and in the
80   greatest water depth of the five cores.

DCR-1PC is the northernmost core and lies in the Subantarctic Zone (SAZ) of the Southern Ocean and is composed of nannofossil and diatom ooze with variable amounts of clay. All other cores predominantly consist of diatom ooze (Kuhn, 2003a, 2003b, 2003c; Oiwane et al., 2014) and lie south of today's position of the Polar Front (PF) in the Antarctic Zone (AZ).

85   **2.2 Age models**

For DCR-1PC, seven ^{14}C-dates were determined and the diatom-based sea surface temperature (SST) record was tuned to the deuterium record of EPICA Dome C, assuming both records are synchronous (Crosta et al., 2020). The stratigraphy for core COR-1bPC is based on 23 calibrated ^{14}C-measurements on planktic foraminifera *neogloboquadrina pachyderma (sinistral)* (Ikehara et al., *in prep.*; Oiwane et al., 2014).
90   For PS2609-1 and PS2606-6 tie points have been established based on graphical alignment of the magnetic susceptibility (MagSus) record to the global benthic $\delta^{18}O$ LR04-stack (Lisiecki and Raymo, 2005). Preliminary alignments were fine-tuned using XRF-scanning iron (Fe), silicon (Si), titanium (Ti), and calcium (Ca) data. For PS2606-6 seven ^{14}C-dates were available (Xiao et al., 2016). Additional tie points were added for core PS2609-1 based on graphical alignment of XRF-scanning Ti measurements with the EPICA Dome C dust record (Lambert et al., 2012), assuming synchronous temporal
95   variability. The Ti- and Ca/Ti-records from PS2606-6 were compared to those of PS2609-1 to define a common stratigraphic

framework (Table 2.1). Our age model was compared to the recently published ^{14}C-based age model of PS2606-6 (Ronge et al., 2020) and both independently determined age models are consistent with one another.

The age model for core PS2603-3 was determined based on graphical alignment of magnetic susceptibility, XRF-data, and biogenic silica with the LR04-stack (Lisiecki and Raymo, 2005). The extinctions of three diatom species served as
100 biostratigraphic markers: *rouxia leventerae* at 130 ka, *hemidiscus karstenii* at 191 ka and *rouxia constricta* at 300 ka (Zielinski and Gersonde, 2002). There is evidence for a 30-ka long hiatus associated with a sediment disturbance close to the MIS 5/4 boundary. Independent absolute age constraints with the constant rate supply (CRS)-model (Geibert et al., 2019) yielded similar ages for PS2603-3, except for the interval around the hiatus.

2.3 Bottom water oxygenation proxies

105 In oxygenated seawater, uranium (U) is present as soluble U(VI). In oxygen-depleted environments however, U is reduced and precipitated as insoluble U(IV) in the form of uraninite (Langmuir, 1978; Morford and Emerson, 1999). Uranium concentrations in sediment porewaters decreases under reducing conditions, creating a concentration gradient between bottom waters and the uppermost sediment layers. This gradient leads to the diffusion of dissolved U into the sediment and to the precipitation of authigenic U (aU) phases (Klinkhammer and Palmer, 1991; Langmuir, 1978).

110 The authigenic fraction of U can be determined by calculating the excess [238]U relative to detrital thorium ([232]Th), by assuming a constant, regionally-informed detrital [238]U/[232]Th ratio. This ratio can vary locally, with lower values generally associated with crustal lithogenic sources. We considered a ratio of 0.5 for cores DCR-1PC, COR-1bPC, PS2909-1, and PS2909-6 (Francois et al., 2004; Henderson and Anderson, 2003). For PS2603-3, the core farthest to the south and potentially influenced by lithogenic material originating from the Antarctic continental crust, the minimum [238]U/[232]Th
115 activity ratio observed is 0.27 ± 0.01. We therefore set the lithogenic end-member conservatively to 0.27.

$$aU = A_{U238}^{total} - A_{Th232}^{total} \times \left(\frac{A_{U238}}{A_{Th232}}\right)^{det} \qquad (1)$$

The U and Th isotope compositions were quantified by isotope dilution following Anderson and Fleer (1982), later modified by Choi et al. (2001), Pichat et al. (2004), and Lippold et al. (2009). Briefly, freeze-dried marine sediments (150–200 mg) were spiked ([229]Th, [236]U) and completely digested in a pressure-assisted microwave ($T_{max} = 180°C$), using concentrated
120 HNO$_3$, HCl and HF. Both elements were separated and purified by anion exchange column chromatography using AG1-X8 resin. Measurements were conducted using a Thermo Fisher Scientific Neptune Plus multi-collector inductively coupled plasma mass spectrometer (MC-ICP-MS) at the University of Bern, and for the PS cores on a single-collector ICP-MS (Thermo Fisher Scientific Element 2) at the Alfred Wegener Institute (AWI) in Bremerhaven. Approximately half of the samples of cores PS2609-1, PS2606-6, and PS2603-3 had been prepared earlier following a similar procedure, albeit with
125 slightly less sediment material (50 mg) and higher temperatures during digestion ($T_{max} = 210°C$). The chromatographic separation and subsequent purification of the U and Th fractions was performed using UTEVA resin (Eichrom). The isotope

measurements were corrected with a calibrated standard (UREM-11 Sarm 31) and yielded a relative standard deviation of less than 3.8 % and 3.5 % for ^{238}U and ^{234}U, and less than 5.7 % and 4.9 % for ^{230}Th and ^{232}Th, respectively. The measurement differences between the two mass spectrometers remain within these error ranges.

130   In marine sediments, manganese (Mn) precipitates under well-oxygenated conditions as oxyhydroxides (Mn(III) and(IV)) (Calvert and Pedersen, 1996). Manganese enrichments in sediments can be observed where the accumulation of organic matter is low and oxic conditions generally prevail (e.g. Calvert and Pedersen, 1993). Under more reducing conditions, the sedimentary distribution of Mn is controlled by the input of insoluble detrital fraction. Any Mn present in the sediment that is in excess relative to the concentration expected from the detrital fraction is assumed to have accumulated authigenically

135   under oxic conditions. Here we use the XRF core scanner peak intensity count ratios between Mn and Ti to constrain excess Mn, assuming a constant detrital ratio between both elements. Ti is assumed to be associated exclusively with lithogenic sources.

For Mn and Ti analyses in cores PS2609-1 and PS2606-6, the samples were fully digested, evaporated and redissolved in 20 ml 1M HNO$_3$. An aliquot was then diluted 1:100 and rhodium as internal standard was added. The Mn and Ti

140   concentrations were measured on the single-collector ICP-MS (Thermo Fisher Scientific Element 2) at AWI in Bremerhaven. Reference material NIST 2702 was digested with each batch and measured with the samples.

For cores COR-1bPC and DCR-1PC, the Mn and Ti measurements were acquired by XRF-core logging with a Tatscan-F2 at the Kochi Core Center, Japan (Sakamoto et al., 2006).

2.4 Preserved opal export

145   The sedimentary biogenic opal fraction is predominantly composed of diatom frustules and minor amounts of radiolarians and sponge spicules. Diatoms dominate carbon export in the Southern Ocean, around and mostly south of the PF (Cortese et al., 2004; Ragueneau, 2000). Sedimentary biogenic silica (bSi), together with other proxies, has been widely used to reconstruct past changes in marine export production (e.g. Anderson et al., 2009; Bradtmiller et al., 2007; Chase et al., 2003). The accumulation of biogenic opal is influenced not only by opal production in the sunlit surface ocean, but also by

150   dissolution in the water column and at the seabed (Dezileau et al., 2003; Pondaven et al., 2000; Ragueneau et al., 2000). Empirical studies of modern opal export patterns suggest that the spatial distribution of opal burial predominantly reflects diatom productivity and opal export (e.g. Chase et al., 2003; Nelson et al., 2002; Pondaven et al., 2000; Sayles et al., 2001). However, the link between opal and carbon export is not straightforward, as other factors such as Fe-availability can affect C and N uptake in diatoms relative to Si (Boutorh et al., 2016; Meyerink et al., 2017; Pichevin et al., 2014). A multi-proxy

155   approach would provide a more unambiguous reconstruction of paleoproductivity in the region. Yet, based on the similar glacial-interglacial patterns of different paleoproductivity proxies in the region (Thöle et al., 2019), we assume that changes in biogenic opal fluxes provide a robust, first-order approximation of past changes in organic carbon delivery to the sediment.

Sedimentary biogenic opal concentrations were determined using Fourier transform infrared spectroscopy (FTIRS) at the

160   University of Bern for cores DCR-1PC and COR-1bPC (Vogel et al., 2016). For the PS cores, the sedimentary opal content
was determined by alkaline extraction of silica according to Müller and Schneider (1993) at AWI, Bremerhaven. Both
methods provide comparable results.

The ^{230}Th-normalization approach was used to reconstruct vertical fluxes of bSi. The methods allows accounting and
correcting for potentially obfuscating effects, such as lateral sediment redistribution by bottom currents (Bourne et al., 2012;

165   Costa et al., 2020; Francois et al., 2004; Henderson and Anderson, 2003). The flux of scavenged ^{230}Th (F^{230}Th) settling to the
seafloor at a specific water depth z is assumed to be equal to its known production rate (β_{230}) from ^{234}U decay within the
water column. The resultant inverse relationship between the scavenged ^{230}Th and the total vertical flux of particulate matter
can be used to calculate preserved vertical fluxes (^{pr}F$_v$) from the activity of initial scavenged ^{230}Th in the sediment
($A^{scav}_{Th230,(0)}$).

170     $$prF_v = \frac{\beta_{230} \times z}{A^{scav}_{Th230,(0)}}$$ (2)

The equation to derive the initial scavenged sedimentary ^{230}Th ($A^{scav}_{Th230,(0)}$) takes into account i) in situ produced ^{230}Th from
the decay of aU (^{238}U); ii) in situ produced ^{230}Th from the decay of lithogenic U (^{238}U); and iii) radiogenic decay of ^{230}Th
after deposition. Normalizing the concentration of a specific sedimentary component (j) with the ^{230}Th-approach provides a
quantitative estimate of its preserved vertical flux (^{pr}F$_j$) through time:

175     $$prF_j = prF_v \times f_j \, ,$$ (3)

where f$_j$ is the weight fraction of constituent j in the sediment.

3 Results

3.1 Subantarctic Zone of the SW Indian Ocean

3.1.1 Redox-sensitive metal records

180   The sedimentary aU concentrations in core DCR-1PC show the highest values of all cores (Figure 2.2). The general pattern
is consistent with a climate-related signal, with typically higher concentrations during cold periods and relatively lower
concentrations during warmer intervals. More specifically, the highest values occur during MIS 6 and MIS 3–2. During
MIS 6 the values decrease gradually, then show a peak around 130 ka, before decreasing steeply to levels well below 1 ppm
at the start of MIS 5. The sedimentary aU concentrations are characterized by transient, millennial-scale oscillations during

185   MIS 5 (106–100 ka, 88–85 ka) and then concentrations increase at the end of MIS 5 and stabilize during MIS 4. At the onset
of MIS 3, aU levels increase steeply, with values remaining high throughout MIS 3, typically ranging between 5 to almost

8 ppm. Authigenic U concentrations start declining after 27 ka and reach the lowest levels of the entire glacial cycle at around 17.5 ka, remaining low throughout the Holocene.

Mn is typically enriched above detritic background values during the two major warm climate intervals of MIS 5 and the
190 Holocene, where values are higher and show increased variability, while Mn/Ti peak intensity count ratios hover around detritic values during cold climate intervals, including a period between 115–100 ka where the values are close to background.

3.1.2 Preserved opal export

Preserved biogenic opal fluxes vary between 0 and 0.7 g cm^{-2} ka^{-1} (Figure 2.2). Opal flux reconstructions show a consistent
195 glacial-interglacial pattern, with typically higher opal fluxes during cold periods and lower fluxes during warmer climate intervals. Biogenic opal fluxes decrease about 5 ka before the onset of the glacial terminations, both during MIS 6 and MIS 2.

There are distinct differences between the downcore aU and bSi flux records. During warm intervals and the transition into MIS 4, both aU and bSi flux records appear to be coupled, but at the start of MIS 3 both parameters start decoupling,
200 suggesting a more complex relation between the two proxies. The Mn/Ti ratio shows an opposing behaviour when compared to aU, with low and stable values during all the periods where aU is elevated, and with higher and more variable values during warmer climate intervals.

3.2 Antarctic Zone of the SW Indian Ocean

3.2.1 Redox-sensitive metal records

205 In the following sections the four cores retrieved from the Antarctic Zone of the Southern Ocean will be described from north to south wherever possible. The downcore sedimentary aU records vary similarly in all four cores (Figure 2.3). Sedimentary concentrations vary between 0 and 3.5 ppm with the southernmost core, PS2603-3, showing the lowest values and generally more subdued temporal variability. The lowest values in all cores are consistently found during MIS 5 and the Holocene. In both PS2609-1 and PS2606-6, there is a pronounced increase in sedimentary aU concentrations during MIS 4.
210 Another increase only clearly visible in PS2609-1 can be found at 85–80 ka. The low values during MIS 3 hover around 1 ppm in PS2609-1 and around 0.5 ppm in PS2606-6, respectively. In COR-1bPC, the core with the shortest sediment record, aU levels start increasing gently from mid MIS 3, before reaching highest values at peak glacial conditions.

The highest aU concentrations in all four cores occur during MIS 2 with a gradual increase from about 30 ka, peaking during the LGM. Thereafter, aU levels decline sharply to values well below 1 ppm within 2–4 ka, concomitant with the onset of the
215 last glacial termination. After TERM I, a small increase around 11–8 ka is apparent. Throughout the Holocene, aU levels stay below 1 ppm.

Authigenic Mn levels remain low throughout the entire ice age and increase at the onset of the last glacial termination. The Mn/Ti records show similar trends with low values during MIS 5 and MIS 4 and elevated or more variable values from about 15 ka.

3.2.2 Preserved opal export

The cores south of the PF show a consistent pattern with relatively low preserved opal fluxes throughout most of MIS 2, 3, and 4, with slight increases and higher variability during MIS 5 and a prominent peak after the LGM. The values reached during this peak are much higher than in the SAZ, with values up to 4 g cm^{-2} ka^{-1}. PS2603-3 shows the overall lowest values, reaching 1.2 g cm^{-2} ka^{-1} after both TERM I and II.

The downcore variations in bSi flux show a very different pattern than the aU records, especially during the LGM and TERM I: simultaneously to the aU decrease, a rapid increase in bSi fluxes at the onset of the last deglaciation is observed. After that, bSi fluxes slowly decrease over the course of the Holocene. During MIS 5 there is a small increase in opal fluxes around 85–75 ka, which seems to coincide with the slightly higher CO_2 levels during MIS 5. The Mn/Ti values remain low in all the cores and rise after the LGM, in parallel with the bSi flux.

4 Interpretation and discussion

4.1 Dynamics of bottom water oxygenation in the SAZ

The downcore aU and Mn/Ti patterns are generally coherent (Figure 2.2), and together the records provide a consistent picture reflecting past changes in oxygenation at the sediment-water interface. Overall the data indicate generally more reducing conditions during cold periods, whereas sediments were more oxidizing during warmer climate intervals. The two redox-sensitive elements however, are not perfectly anti-correlated, consistent with their inherent sensitivities to changing redox conditions (Tribovillard et al., 2006).

When comparing both redox-sensitive metal records to opal fluxes, the proxies broadly agree, in particular at glacial inceptions. But towards peak glacial conditions the records show some degree of divergence.

The first drop in atmospheric pCO$_2$ at around 115 ka marking the glacial inception, coincides with a reduction in Mn/Ti values, which could be attributed to a transition towards more reducing conditions associated with a regional increase in carbon export and sequestration (Figure 2.2). At the transition from MIS 5 to MIS 4, both redox proxies show a clear shift towards more reducing conditions, concomitant with a rise in biogenic opal export, coinciding with a substantial increase in dust, lithogenic and iron deposition rates recorded in Antarctic ice cores (e.g. Lambert et al., 2012) and Subantarctic marine sediments (e.g. Anderson et al., 2014; Lamy et al., 2014; Manoj and Thamban, 2015; Martínez-García et al., 2014; Thöle et al., 2019). Kohfeld and Chase (2017) suggest a major change in ocean circulation, contemporaneous with this second drop in CO$_2$ centered at 72–65 ka. In particular, sedimentary neodymium isotope records and ^{13}C data suggest a major reorganization of deep ocean circulation at that time (e.g. Oliver et al., 2010; Wilson et al., 2015). Indeed, the shoaling of the Atlantic

overturning cell may have left the abyssal ocean dominated by dense southern sourced water (e.g. Lynch-Stieglitz, 2016; Matsumoto et al., 2002), which may have increased the vertical density gradient and contributed to isolate the deep ocean,

250 making it more prone to sequester remineralized carbon (Hain et al., 2010; Skinner, 2009; Yu et al., 2016).

We therefore suggest that both increased export production, and by inference organic matter respiration, as well as a decrease in deep-ocean ventilation (Jaccard et al., 2016) preconditioned the sediments, maintaining sufficiently reducing conditions to allow recording the more subtle ventilation changes of the last ice age (Gottschalk et al., 2020a).

The decrease in aU levels and associated re-oxygenation of bottom waters started within MIS 2 and not, as expected,

255 towards the end of the last ice age, when ocean circulation and upwelling began to intensify as the southern hemisphere warmed (Basak et al., 2018; Gottschalk et al., 2016; Gottschalk et al., 2020b; Jaccard et al., 2016; Rae et al., 2018; Ronge et al., 2020; Skinner et al., 2010). Rather than a regionally disparate initiation of upwelling, the decrease in aU accumulation in core DCR-1PC may be related to diagenetic burn-down. Diagenetic redeposition of sedimentary aU is indeed observed when oxygenated conditions in the uppermost layers of the sediment recur (e.g. Thomson et al., 1990), for example as a result of

260 reinvigorating deep-water ventilation. As oxygen diffuses into pore waters, previously precipitated U will dissolve and will be either lost to the overlying water or diffuse deeper into the sediment, where conditions are still reducing and where it will be reprecipitated (Colley et al., 1989; Jacobel et al., 2017; Mangini et al., 2001). A high sediment accumulation rate would limit the depth interval over which burn-down would affect the downcore aU record. Core DCR-1PC has the lowest sedimentation rates of the five cores investigated and thus is potentially more prone to be affected by oxidative burn-down.

265 With the lowest sedimentation rate within the core being reported between 17 ka and 25 ka (<1 cm ka^{-1}, Figure 2.4), re-dissolution provides a plausible explanation accounting for the early aU decrease.

During the penultimate glacial termination (TERM II), aU appears to have only been marginally affected by remobilization processes. The sedimentation rates during this interval are indeed higher than at the end of the last ice age (Figure 2.4). The distinct peaks preceding the rapid decrease in aU are a possible indicator for some degree of burn-down at both terminations

270 (Colley et al., 1989).

The early decrease in bSi export towards the end of both glacial periods could be related to increasingly complete $Si(OH)_4$ consumption south of the Polar Front (Dumont et al., 2020). Upwelling and thus nutrient supply to the surface water south of the PF were substantially reduced during glacial times (Anderson et al., 2009; Francois et al., 1997). Biological productivity was reduced, but at the same time nitrate consumption was more complete (Ai et al., 2020; Studer et al., 2015), stemming

275 CO_2 outgassing from the ocean interior. Part of these surface waters are transported towards the north and when they reach the location of DCR-1PC, they are largely depleted in $Si(OH)_4$. Transitioning towards peak glacial conditions there would have been gradually less $Si(OH)_4$ available for opal production in the SAZ, as reflected by the downcore opal flux records. Relaxed Fe-limitation as a result of enhanced bioavailable Fe-input with dust would have lowered the Si:N uptake ratio in diatoms (Brzezinski et al., 2002). Nitrogen isotope studies show that nitrate utilization was more complete in glacial periods

280 when compared to interglacials (Ai et al., 2020; Horn et al., 2011; Martínez-García et al., 2014; Studer et al., 2015), whereas silicon isotopes show an opposite pattern (Brzezinski et al., 2002; Dumont et al., 2020). Despite preferred nitrate uptake and

therefore potentially more silicate leakage towards the north, the overall amount of Si(OH)$_4$ upwelled from depth might have been declining, thus limiting diatom growth (Brzezinski et al., 2002; Dumont et al., 2020).

Moreover, a migration of the frontal system cannot be ruled out as a potential explanation for the early reduction in opal

285   fluxes. DCR-1PC today is located not only north of the Polar Front, but also north of the Subantarctic Front (Orsi et al., 1995; Pollard et al., 2007). A possible explanation for the opal flux decrease within MIS 2 relates to the northward displacement of the fronts so that the core location lies in the Polar Frontal Zone, where during MIS 2 nutrient availability was possibly reduced.

4.2 Dynamics of bottom water oxygenation in the AZ

290   South of the PF, all of the cores, with the exception of the slowly accumulating core retrieved from Enderby Basin, record similar (paleo)oceanographic dynamics. The sedimentary aU and Mn/Ti levels show a consistent downcore pattern with generally more reducing conditions during peak glacial times and rapid reoxygenation during glacial terminations, broadly similar to the SAZ record. The somewhat noisy Mn/Ti signal from 15 ka onwards, especially in COR-1bPC, suggests transient variability in bottom water oxygenation. Recorded opal fluxes are persistently low during cold periods, while aU

295   and Mn/Ti values are consistent with increasingly reducing conditions. The rapid increase of preserved opal fluxes coinciding with more oxygenated conditions during TERM I imply that export production and thus the respiratory demand for organic matter remineralization only plays a secondary role, whereas ventilation imposes a primary control on sedimentary oxygenation levels.

The rapid increase of biogenic opal fluxes at the onset of both glacial terminations is likely a result of enhanced upwelling of

300   subsurface waters, rich in both (micro)nutrients and CO$_2$ (Anderson et al., 2009; Gottschalk et al., 2020b; Jaccard et al., 2016; Skinner et al., 2010). The bSi flux values of the peak at TERM I suggest that COR-1bPC was closest to the most vigorous upwelling location at the onset of deglaciation.

With the available data of redox-sensitive elements U and Mn and the preserved opal fluxes in these cores, an alternative interpretation needs to be considered. As Fe-scarcity reduces the C and N uptake ratio relative to Si (Boutorh et al., 2016;

305   Meyerink et al., 2017; Pichevin et al., 2014), the opal peak during the deglaciation can at least partly be attributed to Fe-limitation, possibly induced by a reduction of Fe-bearing dust input. To further explore this alterative possibility, downcore changes in Si/Fe ratios in diatom shells could be analyzed. However, considering multi-proxy studies of export production in the AZ (e.g. Chase et al., 2003; Thöle et al., 2019) and enhanced upwelling intensities during the deglacial (e.g. Basak et al., 2018; Gottschalk et al., 2020b; Ronge et al., 2020; Skinner et al., 2010), we suggest the observed opal peak to be the result of

310   increased production due to enhanced nutrient availability from upwelled deep waters, in line with a meridional shift of the Southern Ocean frontal system.

Reinvigorating ventilation in the Southern Ocean associated with the glacial termination would leave a spatially coherent oxygenation pattern in all cores, as it was related to an overall reorganization in ocean circulation. The associated opal signal might slightly differ in time given that the upwelling region shifts along with the frontal system (Anderson et al., 2009).

315   However, the sampling resolution is insufficient to reliably assess the potential time lag between the onset of the aU decrease and the sharp rise of opal production and deposition.

The slight increase in aU concentrations midway through the deglaciation could reflect a transient slowdown in ventilation associated with the Antarctic Cold Reversal (ACR) (Jaccard et al., 2016), notwithstanding age model uncertainties. The concomitant increase in Mn/Ti, which indicates a more oxidizing environment, can be explained by different sensitivities of
320   the two elements to redox changes.

In the southernmost core PS2603-3, aU and preserved opal fluxes suggest similar oceanographic dynamics in the Enderby Abyssal Plain. The opal peak concomitant with the onset of TERM I suggests that the core is similarly recording enhanced upwelling, yet the maximum values of 1.2 g cm^{-2} ka^{-1} are consistent with the core being located further away from the most vigorous upwelling region. The slight increase in the aU record during the glacial maxima suggests that bottom water
325   oxygenation was generally reduced during ice ages.

4.3 Ventilation and circulation changes on glacial-interglacial timescales and their impact on atmospheric pCO$_2$

Across the sampled transect, the core site locations are bathed by different water masses. With the exception of the southernmost core, which is currently bathed by Antarctic Bottom Water (AABW), the other four sediment cores are located in Circumpolar Deep Water (CDW), which is formed partly from North Atlantic Deep Water (NADW), mixed with AABW
330   and other deep waters that originate from the Indian and Pacific oceans (Talley, 2013). CDW is upwelled in the Southern Ocean along tilted isopycnals. The lower CDW, which stems mainly from dense, high salinity NADW, then moves towards the south as a precursor for AABW. The less dense upper CDW, which has a more oxygen-depleted signature from older Indian and Pacific deep waters, is transported to the north by Ekman flow (Talley, 2013). The lower and upper CDW thus have distinct oxygen concentrations, but the range in dissolved oxygen concentration changes is smaller than the ranges
335   reported for the last glacial cycle due to increased carbon sequestration as has previously been suggested (Anderson et al., 2019; Galbraith and Skinner, 2020). Therefore, any variations in aU and Mn/Ti values are unlikely to be primarily driven by local variations in oxygenation, but rather represent a coherent regional picture.

As discussed above, export production is unlikely to have played a dominant role in modulating past changes in bottom water oxygenation and especially south of the PF, it is of secondary importance. The main factor controlling changes in
340   oxygenation at the sediment-water interface is thus more likely related to bottom water ventilation changes. This can be argued by the decoupling of aU and opal fluxes in DCR-1PC during the later phase of the glacial periods and by the more pronounced antiphasing in the records south of the PF. This antiphasing at TERM I with invigorated circulation and thus rejuvenation of the deep ocean is linked to enhanced supply of nutrient-rich waters to the surface, which fueled biological production. However, this nutrient-fueled phytoplankton growth was not efficient to quantitatively fix dissolved carbon, thus
345   allowing CO$_2$ to escape to the atmosphere (Ai et al., 2020; Sigman et al., 2010; Studer et al., 2015). The increase in opal fluxes in connection with more ventilated bottom waters at the end of the glacial periods fits well with higher atmospheric

CO$_2$ inventories associated with the release of previously sequestered carbon from subsurface waters (Burke and Robinson, 2012; Jaccard et al., 2016; Ronge et al., 2020; Skinner et al., 2010).

The major slowdown in deep ocean circulation occurred mostly after the MIS 5/4 transition. Before, at the onset of the
350   glacial period, other factors may have contributed to the drawdown of atmospheric carbon. During the first CO$_2$ drop within MIS 5, cooling sea surface temperatures at high latitudes of both hemispheres led to CO$_2$ reduction through barrier mechanisms. Sea-ice formation and seasonally induced melt water would lead to stronger surface water stratification and affect air-sea gas exchange and impede lower waters to rise to the productive surface (Watson and Naveira Garabato, 2006; Wolff et al., 2010). This barrier mechanism is consistent with the observed first increase in nitrate consumption associated
355   with enhanced stratification of the surface ocean (Ai et al., 2020; Studer et al., 2015). Only at the second CO$_2$ drop at the MIS 5/4 transition would deep ocean circulation slow, as is indicated by increased aU and decreased Mn/Ti and in good agreement with other proxy data (Jimenez-Espejo et al., 2020; Kohfeld and Chase, 2017; Oliver et al., 2010; Wilson et al., 2015). This second drop was accompanied by enhanced biological export production north of the PF fueled by enhanced dust input (Lambert et al., 2012). Our results showing a regionally coherent increase in sedimentary aU concentrations,
360   especially after the MIS 5/4 transition, indicate gradually more sluggish overturning circulation that contributed to partitioning carbon into the ocean interior (Gottschalk et al., 2020a; Jaccard et al., 2016, 2013; Kohfeld and Chase, 2017).

South of the PF in core PS2609-1 the aU record indicates re-oxygenation during MIS 3, while in the SAZ reducing conditions intensify. This contrasting behavior could be explained by a reorganization of deep-water masses. NADW that forms CDW in which our cores are located in modern times could have retracted northwards during MIS 3, while AAWB,
365   generally more oxygenated than NADW, bathed the cores south of the PF (Sigman et al., 2010). Progressing towards the glacial maximum, the upwelled water masses would successively be more isolated from atmospheric forcing by extended sea-ice, leading to more oxygen-depleted and carbon rich AABW (Ferrari et al. 2014), and thus resulting in the increased aU levels in the southern cores during MIS 2.

5 Conclusions

370   Five marine sediment cores from the Indian sector of the Southern Ocean were analyzed in this study. They were retrieved across a transect spanning a latitudinal band of about 15° from Del Caño Rise, north of the SAF, over Conrad Rise and as far south as the Enderby Abyssal Plain, close to the Southern ACC Front (SACCF). Redox-sensitive aU and Mn/Ti XRF peak intensity count ratios were studied in detail and compared to [230]Th-normalized preserved opal export fluxes to better constrain bottom water oxygenation in the context of carbon sequestration since the last glacial inception. Our results suggest
375   that more sluggish circulation dynamics and thus ventilation changes are the major contributor accounting for enhanced carbon sequestration in deep-water masses during glacial periods. Our paleoceanographic records covering a meridional transect increase the spatial resolution of deep-water oxygenation records in the Southern Ocean and are overall in agreement

with previous reconstructions from other deep-water sites (Chase et al., 2001; Dezileau et al., 2002; Francois et al., 1997; Frank et al., 2000; Gottschalk et al., 2020b; Jaccard et al., 2016; Thöle et al., 2019).

380 The influence of locally enhanced biological export production on oxygenation states due to increased Fe-fertilization by dust input cannot be ruled out completely, especially in the SAZ and at the transition from MIS 5 to 4 (Jaccard et al., 2016, 2013; Martínez-García et al., 2014). In the AZ however, export production likely played a minor role in partitioning carbon from the atmosphere. More importantly, decreased ventilation and the associated slowdown of overall ocean circulation during cold periods led to more carbon being sequestered in the ocean interior. Our results indicate a major drawdown of

385 atmospheric CO_2 by a more sluggish overturning circulation. The most substantial circulation changes are suggested to have occurred at the transition of MIS 5/4 as has been proposed by Kohfeld and Chase (2017).

South of the PF, reducing conditions recede during MIS 3, most likely due to a reorganization of deep-water circulation with larger expansion of AABW, reaching the southern core locations (Ferrari et al., 2014). Later during MIS 2, also these deep waters, that upwell to newly form AABW, were increasingly isolated from atmospheric forcing due to expanded sea ice

390 cover.

Generally, our reconstructions support the hypothesis that ventilation dynamics are the main driver of oxygenation changes in the Southern Ocean and thus exert the major control on the air-sea partitioning of CO_2 over the last glacial cycle.

Author contribution

HEA and SLJ designed the study. HEA, LMT, IS, and WG carried out U/Th measurements and evaluation. HEA and GK

395 carried out biogenic opal measurements. IS and WG conducted the absolute Mn and Ti measurements. MI and GK planned the cruises and gave access to the cores and to XRF-measurements. MI, OE, and HEA obtained tiepoints to develop and refine the age models. HEA wrote the initial version of the manuscript and all co-authors contributed to the manuscript.

Competing interests

The authors declare that they have no conflict of interest.

400 **Acknowledgement**

We thank the captain, crew members and scientists of the R/V *Hakuho-maru* and R/V *Polarstern* for the recovery of the sediment cores during KH-10-7 (lead scientist: M. Ikehara) and ANT-XI/4 cruises (lead scientist: G. Kuhn) to the Southern Ocean. We thank Martin Wille, Igor Villa, Jörg Rickli, David Janssen, Edel O'Sullivan, Alessandro Maltese, and Jörg Lippold for their help with the MC-ICP-MS measurements, Julijana Krbanjevic and Hendrik Vogel for helping with the opal

405 measurements, and Takuya Matsuzaki for the Tatscan measurements. Funding for this study was provided by the Swiss

National Science Foundation (grants PP00P2_144811 and 2000021_163003). O. Esper, W. Geibert, G. Kuhn and I. Stimac were funded by the Alfred-Wegener-Institut Helmholtz-Zentrum für Polar- und Meeresforschung PACES II research program. M. Ikehara was funded by the Japan Society for the Promotion of Science KAKENHI (Grants-in-Aid for Scientific Research P23244102 and JP17H06318). The isotope data was obtained on a Neptune MC-ICP-mass spectrometer acquired
410   with funds from the NCCR PlanetS supported by the Swiss National Science Foundation grant no. 51NF40-141881.

References

Adkins, J. F.: The role of deep ocean circulation in setting glacial climates, Paleoceanography, 28, 539–561, doi:10.1002/palo.20046, 2013.

Adkins, J. F., McIntyre, K., and Schrag, D. P.: The salinity, temperature, and δ18O of the glacial deep ocean, Science, 298,
415   69–73, doi:10.1126/science.1076252, 2002.

Ai, X. E., Studer, A. S., Sigman, D. M., Martínez-García, A., Fripiat, F., Thöle, L. M., Michel, E., Gottschalk, J., Arnold, L., Moretti, S, Schmitt, M., Oleynik, S., Jaccard, S. L., and Haug, G. H.: Southern Ocean upwelling, Earth's obliquity, and glacial-interglacial atmospheric CO_2 change, Science, 370, 6522, 1348–1352, doi:10.1126/science.abd2115, 2020.

Anderson, R. F., Ali, S., Bradtmiller, L. I., Nielsen, S. H. H., Fleisher, M. Q., Anderson, B. E., and Burckle, L. H.: Wind-
420   driven Upwelling in the Southern Ocean and the Deglacial Rise in Atmospheric CO_2, Science, 323, 1443–1448, doi:10.1126/science.1167441, 2009.

Anderson, R. F., Barker, S., Fleisher, M., Gersonde, R., Goldstein, S. L., Kuhn, G., Mortyn, P. G., Pahnke, K., and Sachs, J. P.: Biological response to millennial variability of dust and nutrient supply in the Subantarctic South Atlantic Ocean, Philos. Trans. R. Soc. A, 372, 20130054, doi:10.1098/rsta.2013.0054, 2014.

425   Anderson, R. F. and Fleer, A. P.: Determination of Natural Actinides and Plutonium in Marine Particulate Material, Anal. Chem. 54, 1142–1147, doi:10.1021/ac00244a030, 1982.

Anderson, R. F., Sachs, J. P., Fleisher, M. Q., Allen, K. A., Yu, J., Koutavas, A., and Jaccard, S. L.: Deep-sea oxygen depletion and ocean carbon sequestration during the last ice age, Global Biogeochem. Cycles, 33, 301–317, doi:10.1029/2018GB006049, 2019.

430   Basak, C., Fröllje, H., Lamy, F., Gersonde, R., Benz, V., Anderson, R. F., Molina-Kescher, M., and Pahnke, K.: Breakup of last glacial deep stratification in the South Pacific, Science, 359, 900–904, doi:10.1126/science.aao2473, 2018.

Bauska, T. K., Baggenstos, D., Brook, E. J., Mix, A. C., Marcott, S. E., Petrenko, V. V., Schaefer, H., Severinghaus, J. P., and Lee, J. E.: Carbon isotopes characterize rapid changes in atmospheric carbon dioxide during the last deglaciation, Proc. Nat. Acad. Sci., doi:10.1073/pnas.1513868113, 2016.

435   Bereiter, B., Eggleston, S., Schmitt, J., Nehrbass-Ahles, C., Stocker, T. F., Fischer, H., Kipfstuhl, S., and Chappellaz, J.: Revision of the EPICA Dome C CO_2 record from 800 to 600 kyr before present, Geophys. Res. Lett., 42, 542–549, doi:10.1002/2014GL061957, 2015.

Bourne, M. D., Thomas, A. L., Mac Niocaill, C., and Henderson, G. M.: Improved determination of marine sedimentation rates using $^{230}Th_{xs}$, Geochemistry, Geophys. Geosystems, 13, 1, doi:10.1029/2012GC00429, 2012.

440 Boutorh, J., Moriceau, B., Gallinari, M., Ragueneau, O., and Bucciarelli, E.: Effect of trace metal-limited growth on the postmortem dissolution of the marine diatom Pseudo-nitzschia delicatissima, Global Biogeochem. Cycles, 30, 57–69, doi:10.1002/2015GB005088, 2016.

Bouttes, N., Paillard, D., and Roche, D. M.: Impact of brine-induced stratification on the glacial carbon cycle, Clim. Past, 6, 575–589, doi:10.5194/cp-6-575-2010, 2010.

445 Bradtmiller, L. I., Anderson, R. F., Fleisher, M. Q., and Burckle, L. H.: Opal burial in the equatorial Atlantic Ocean over the last 30 ka: Implications for glacial-interglacial changes in the ocean silicon cycle, Paleoceanography, 22, PA4216, 1–15, doi:10.1029/2007PA001443, 2007.

Brzezinski, M. A., Pride, C. J., Franck, V. M., Sigman, D. M., Matsumoto, K., Gruber, N., Rau, G. H., and Coale, K. H.: A switch from $Si(OH)_4$ to NO_3^- depletion in the glacial Southern Ocean, Geophys. Res. Lett., 29, 12, 1564,
450 doi:10.1029/2001GL014349, 2002.

Burke, A. and Robinson, L. F.: The Southern Ocean's Role in Carbon Exchange During the Last Deglaciation, Science, 335, 557–561, doi:10.1126/science.1208163, 2012.

Calvert, S. E. and Pedersen, T. F.: Geochemistry of Recent oxic and anoxic marine sediments: Implications for the geological record, Mar. Geol., 113, 67–88, doi:10.1016/0025-3227(93)90150-T, 1993.

455 Calvert, S. E. and Pedersen, T. F.: Sedimentary geochemistry of manganese: Implications for the environment of formation of manganiferous black shales, Econ. Geol., 91, 36–47, doi:10.2113/gsecongeo.91.1.36, 1996.

Chase, Z., Anderson, R. F., and Fleisher, M. Q.: Evidence from authigenic uranium for increased productivity of the glacial Subantarctic Ocean, Paleoceanography, 16, 5, 468–478, doi:10.1029/2000PA000542, 2001.

Chase, Z., Anderson, R. F., Fleisher, M. Q., and Kubik, P. W.: Accumulation of biogenic and lithogenic material in the
460 Pacific sector of the Southern Ocean during the past 40,000 years, Deep. Res. Part II Top. Stud. Oceanogr, 50, 799–832, doi:10.1016/S0967-0645(02)00595-7, 2003.

Choi, M. S., Francois, R., Sims, K., Bacon, M. P., Brown-Leger, S., Fleer, A. P., Ball, L., Schneider, D., and Pichat, S.: Rapid determination of ^{230}Th and ^{231}Pa in seawater by desolvated micro-nebulization Inductively Coupled Plasma magnetic sector mass spectrometry, Mar. Chem., 76, 99–112, doi:10.1016/S0304-4203(01)00050-0, 2001.

465 Colley, S., Thomson, J., and Toole, J.: Uranium relocations and derivation of quasi-isochrons for a turbidite/pelagic sequence in the Northeast Atlantic, Geochim. Cosmochim. Acta, 53, 1223–1234, doi:10.1016/0016-7037(89)90058-6, 1989.

Cortese, G., Gersonde, R., Hillenbrand, C. D., and Kuhn, G.: Opal sedimentation shifts in the World Ocean over the last 15 Myr, Earth Planet. Sci. Lett., 224, 509–527, doi:10.1016/j.epsl.2004.05.035, 2004.

Costa, K. M., Hayes, C. T., Anderson, R. F., Pavia, F. J., Bausch, A., Deng, F., Dutay, J. C., Geibert, W., Heinze, C.,
470 Henderson, G., Hillaire-Marcel, C., Hoffmann, S., Jaccard, S. L., Jacobel, A. W., Kienast, S. S., Kipp, L., Lerner, P., Lippold, J., Lund, D., Marcantonio, F., McGee, D., McManus, J. F., Mekik, F., Middleton, J. L., Missiaen, L., Not, C.,

Pichat, S., Robinson, L. F., Rowland, G. H., Roy-Barman, M., Tagliabue, A., Torfstein, A., Winckler, G., and Zhou, Y.: [230]Th normalization: New insights on an essential tool for quantifying sedimentary fluxes in the modern and Quaternary ocean, Paleoceanogr. Paleoclimatology, 35, e2019PA003820, 1–36, doi:10.1029/2019PA003820, 2020.

475   Crosta, X., Shukla, S. K., Ther, O., Ikehara, M., Yamane, M., and Yokoyama, Y.: Last Abundant Appearance Datum of Hemidiscus karstenii driven by climate change, Mar. Micropaleontol., 157, doi:10.1016/j.marmicro.2020.101861, 2020.

Dezileau, L., Bareille, G., and Reyss, J.-L.: Enrichissement en uranium authigène dans les sédiments glaciaires de l'océan Austral, C. R. Geoscience, 334, 1039–1046, doi:10.1016/S1631-0713(02)01826-6, 2002.

Dezileau, L., Reyss, J.-L., and Lemoine, F.: Late Quaternary changes in biogenic opal fluxes in the Southern Indian Ocean,
480   Mar. Geol., 202, 143–158, doi:10.1016/S0025-3227(03)00283-4, 2003.

Dumont, M., Pichevin, L., Geibert, W., Crosta, X., Michel, E., Moreton, S., Dobby, K., and Ganeshram, R.: The nature of deep overturning and reconfigurations of the silicon cycle across the last deglaciation, Nat. Commun., 11, 1534, doi:10.1038/s41467-020-15101-6, 2020.

Ferrari, R., Jansen, M. F., Adkins, J. F., Burke, A., Stewart, A. L., and Thompson, A. F.: Antarctic sea ice control on ocean
485   circulation in present and glacial climates, Proc. Natl. Acad. Sci. U. S. A., 111, 24, 8753–8758, doi:10.1073/pnas.1323922111, 2014.

Francois, R., Altabet, M. A., Yu, E.-F., Sigman, D. M., Bacon, M. P., Frank, M., Bohrmann, G., Bareille, G., and Labeyrie, L. D.: Contribution of Southern Ocean surface-water stratification to low atmospheric CO_2 concentrations during the last glacial period, Nature, 389, 6654, 929–935, doi:10.1038/40073, 1997.

490   Francois, R., Frank, M., Rutgers van der Loeff, M. M., and Bacon, M. P.: [230]Th normalization: An essential tool for interpreting sedimentary fluxes during the late Quaternary, Paleoceanography, 19, PA1018, doi:10.1029/2003pa000939, 2004.

Frank, M., Gersonde, R., Rutgers van der Loeff, M. M., Bohrmann, G., Nürnberg, C. C., Kubik, P. W., Suter, M., and Mangini, A.: Similar glacial and interglacial export bioproductivity in the Atlantic sector of the Southern Ocean: Multiproxy
495   evidence and implications for glacial atmospheric CO_2, Paleoceanography, 15, 6, 642–658, doi:10.1029/2000PA000497, 2000.

Galbraith, E. D. and Jaccard, S. L.: Deglacial weakening of the oceanic soft tissue pump: Global constraints from sedimentary nitrogen isotopes and oxygenation proxies, Quat. Sci. Rev., 109, 38–48, doi:10.1016/j.quascirev.2014.11.012, 2015.

500   Galbraith, E. D. and Skinner, L.C.: The Biological Pump During the Last Glacial Maximum, Annual Review of Marine Science, 12, 559–586, doi:10.1146/annurev-marine-010419-010906, 2020.

Galbraith, E. D., Young Kwon, E., Bianchi, D., Hain, M. P., and Sarmiento, J. L.: The impact of atmospheric pCO_2 on carbon isotope ratios of the atmosphere and ocean, Global Biogeochem. Cycles, 29, 307–324, doi:10.1002/2014GB004929, 2015.

505   Geibert, W., Stimac, I., Rutgers van der Loeff, M. M., and Kuhn, G.: Dating Deep-Sea Sediments With [230]Th Excess Using a Constant Rate of Supply Model, Paleoceanogr. Paleoclimatology, 34, 1895–1912, doi:10.1029/2019PA003663, 2019.

Gottschalk, J., Skinner, L. C., Lippold, J., Vogel, H., Frank, N., Jaccard, S. L., and Waelbroeck, C.: Biological and physical controls in the Southern Ocean on past millennial-scale atmospheric CO_2 changes, Nat. Commun., 7, doi:10.1038/ncomms11539, 2016.

510   Gottschalk, J., Skinner, L. C., Jaccard, S. L., Menviel, L., Nehrbass-Ahles, C., and Waelbroeck, C.: Southern Ocean link between changes in atmospheric CO_2 levels and northern-hemisphere climate anomalies during the last two glacial periods, Quat. Sci. Rev., 230, 106067, doi:10.1016/j.quascirev.2019.106067, 2020a.

Gottschalk, J., Michel, E., Thöle, L. M., Anja S. Studer, A. S., Hasenfratz, A. P., Schmid, N., Butzin, M., Mazaud, A., Martínez-García, A., Szidat, S., and Jaccard, S. L.: Glacial heterogeneity in Southern Ocean carbon storage abated by fast

515   South Indian deglacial carbon release, Nat. Commun., 11:6192, doi:10.1038/s41467-020-20034-1, 2020b.

Hain, M. P., Sigman, D. M., and Haug, G. H.: Carbon dioxide effects of Antarctic stratification, North Atlantic Intermediate Water formation, and subantarctic nutrient drawdown during the last ice age: Diagnosis and synthesis in a geochemical box model, Global Biogeochem. Cycles, 24, GB4023, 1–19, doi:10.1029/2010GB003790, 2010.

Henderson, G. M.: Seawater ($^{234}U/^{238}U$) during the last 800 thousand years, Earth Planet. Sci. Lett., 6183, 1–14,

520   doi:10.1016/S0012-821X(02)00556-3, 2002.

Henderson, G. M. and Anderson, R. F.: The U-series toolbox for paleoceanography, Rev. Mineral. Geochemistry, 52, 493–531, doi:10.2113/0520493, 2003.

Hoogakker, B. A. A., Elderfield, H., Schmiedl, G., McCave, I. N., and Rickaby, R. E. M.: Glacial–interglacial changes in bottom-water oxygen content on the Portuguese margin, Nat. Geosci., 8, 2–5, doi:10.1038/ngeo2317, 2015.

525   Horn, M. G., Robinson, R. S., Rynearson, T. A., and Sigman, D. M.: Nitrogen isotopic relationship between diatom-bound and bulk organic matter of cultured polar diatoms, Paleoceanography, 26, PA3208, doi:10.1029/2010PA002080, 2011.

Ikehara, M., Katsuki, K., Yamane, M., Yokoyama, Y., Obrochta, S. P., Matsuzaki, T., Sato, H., and Kusahara, K., (in prep.). Episodic enhancement of sea ice survivability in the glacial Southern Ocean driven by Antarctic warming.

Jaccard, S. L., Hayes, C. T., Hodell, D. A., Anderson, R. F., Sigman, D. M., and Haug, G. H.: Two modes of change in SO

530   Productivity, Science, 339, 6126, 1419–1423, doi:10.1126/science.1227545, 2013.

Jaccard, S. L., Galbraith, E. D., Martínez-García, A., and Anderson, R. F.: Covariation of deep Southern Ocean oxygenation and atmospheric CO_2 through the last ice age, Nature, 530, 207–210, doi:10.1038/nature16514, 2016.

Jacobel, A. W., McManus, J. F., Anderson, R. F., and Winckler, G.: Repeated storage of respired carbon in the equatorial Pacific Ocean over the last three glacial cycles, Nat. Commun., 8, doi:10.1038/s41467-017-01938-x, 2017.

535   Jimenez-Espejo, F. J., Presti, M., Kuhn, G., McKay, R., Crosta, X., Escutia, C., Lucchi, R. G., Tolotti, R., Yoshimura, T., Ortega Huertas, M., Macrì, P., Caburlotto, A., and De Santis, L.: Late Pleistocene oceanographic and depositional variations along the Wilkes Land margin (East Antarctica) reconstructed with geochemical proxies in deep-sea sediments, Glob. Planet. Change, 184, 103045, doi:10.1016/j.gloplacha.2019.103045, 2020.

Jouzel, J., Masson-Delmotte, V., Cattani, O., Dreyfus, G., Falourd, S., Hoffmann, G., Minster, B., Nouet, J., Barnola, J. M.,
540   Chappellaz, J., Fischer, H., Gallet, J.C., Johnsen, S., Leuenberger, M., Loulergue, L., Luethi, D., Oerter, H., Parrenin, F.,
Raisbeck, G., Raynaud, D., Schilt, A., Schwander, J., Selmo, E., Souchez, R., Spahni, R., Stauffer, B., Steffensen, J. P.,
Stenni, B., Stocker, T. F., Tison, J. L., Werner, M., and Wolff, E. W.: Orbital and millennial antarctic climate variability over
the past 800,000 years, Science, 317, 5839, 793–796, doi:10.1126/science.1141038, 2007.

Klinkhammer, G. P. and Palmer, M. R.: Uranium in the oceans: Where it goes and why, Geochim. Cosmochim. Acta, 55,
545   1799–1806, doi:10.1016/0016-7037(91)90024 Y, 1991.

Kohfeld, K. E. and Chase, Z.: Temporal evolution of mechanisms controlling ocean carbon uptake during the last glacial
cycle, Earth Planet. Sci. Lett., 472, 206–215, doi:10.1016/j.epsl.2017.05.015, 2017.

Kohfeld, K. E., Le Quéré, C., Harrison, S. P., and Anderson, R. F.: Role of marine biology in glacial-interglacial CO_2 cycles,
Science, 308, 74–78, doi:10.1126/science.1105375, 2005.

550   Kuhn, G.: Documentation of sediment core PS2609-1, Alfred Wegener Institute - Polarstern core repository, PANGAEA,
doi:10.1594/PANGAEA.115378, 2003a.

Kuhn, G.: Documentation of sediment core PS2606-6, Alfred Wegener Institute - Polarstern core repository, PANGAEA,
doi:10.1594/PANGAEA.115376, 2003b.

Kuhn, G.: Documentation of sediment core PS2603-3, Alfred Wegener Institute - Polarstern core repository, PANGAEA,
555   doi:10.1594/PANGAEA.115375, 2003c.

Kumar, N., Anderson, R. F., Mortlock, R. A., Froelich, P. N., Kubik, P., Dittrich-Hannen, B., and Suter, M.: Increased
biological production and export in the glacial Southern Ocean, Nature, 378, 675–680, doi:10.1038/378675a0, 1995.

Lambert, F., Bigler, M., Steffensen, J. P., Hutterli, M., and Fischer, H.: Centennial mineral dust variability in high-resolution
ice core data from Dome C, Antarctica, Clim. Past, 8, 609–623, doi:10.5194/cp-8-609-2012, 2012.

560   Lamy, F., Gersonde, R., Winckler, G., Esper, O., Jaeschke, A., Kuhn, G., Ullermann, J., Martínez-García, A., Lambert, F.,
and Kilian, R.: Increased dust deposition in the Pacific Southern Ocean during glacial periods, Science, 343, 403–407,
doi:10.1126/science.1245424, 2014.

Langmuir, D.: Uranium solution-mineral equilibria at low temperatures with applications to sedimentary ore deposits,
Geochim. Cosmochim. Acta, 42, 547–569, doi:10.1016/0016-7037(78)90001-7, 1978.

565   Lippold, J., Grützner, J., Winter, D., Lahaye, Y., Mangini, A., and Christi, M.: Does sedimentary ^{231}Pa/^{230}Th from the
Bermuda Rise monitor past Atlantic Meridional Overturning Circulation?, Geophys. Res. Lett., 36, L12601, 1–6,
doi:10.1029/2009GL038068, 2009.

Lisiecki, L. E. and Raymo, M. E.: A Pliocene-Pleistocene stack of 57 globally distributed benthic δ^{18}O records,
Paleoceanography, 20, PA1003, 1–17, doi:10.1029/2004PA001071, 2005.

570   Lynch-Stieglitz, J., Ito, T., and Michel, E.: Antarctic density stratification and the strength of the circumpolar current during
the Last Glacial Maximum, Paleoceanography, 31, 539–552, doi:10.1002/2015PA002915, 2016.

Mangini, A., Jung, M., and Laukenmann, S.: What do we learn from peaks of uranium and of manganese in deep sea sediments?, Mar. Geol., 177, 63–78, doi:10.1016/S0025-3227(01)00124-4, 2001.

Manoj, M. C. and Thamban, M.: Shifting frontal regimes and its influence on bioproductivity variations during the Late
575 Quaternary in the Indian sector of Southern Ocean, Deep. Res. Part II Top. Stud. Oceanogr., 118, 261–274, doi:10.1016/j.dsr2.2015.03.011, 2015.

Marshall, J. and Speer, K.: Closure of the meridional overturning circulation through Southern Ocean upwelling, Nat. Geosci., 5, 171–180, doi:10.1038/ngeo1391, 2012.

Martínez-García, A., Sigman, D. M., Ren, H., Anderson, R. F., Straub, M., Hodell, D. A., Jaccard, S. L., Eglinton, T. I., and
580 Haug, G. H.: Iron fertilization of the subantarctic ocean during the last ice age, Science, 343, 1347–1350, doi:10.1126/science.1246848, 2014.

Matsumoto, K., Sarmiento, J. L., and Brzezinski, M. A.: Silicic acid leakage from the Southern Ocean: A possible explanation for glacial atmospheric pCO$_2$, Global Biogeochem. Cycles, 16, 3, 1031, doi:10.1029/2001GB001442, 2002.

Meyerink, S. W., Ellwood, M. J., Maher, W. A., Dean Price, G., and Strzepek, R. F.: Effects of iron limitation on silicon
585 uptake kinetics and elemental stoichiometry in two Southern Ocean diatoms, Eucampia antarctica and Proboscia inermis, and the temperate diatom Thalassiosira pseudonana, Limnol. Oceanogr., 62, 6, 2445–2462, doi:10.1002/lno.10578, 2017.

Morford, J. L. and Emerson, S.: The geochemistry of redox sensitive trace metals in sediments, Geochim. Cosmochim. Acta, 63, 1735–1750, doi:10.1016/S0016-7037(99)00126-X, 1999.

Müller, P. J. and Schneider, R.: An automated leaching method for the determination of opal in sediments and particulate
590 matter, Deep. Res. Part I, 40, 3, 425–444, doi:10.1016/0967-0637(93)90140-X, 1993.

Nameroff, T. J., Balistrieri, L. S., and Murray, J. W.: Suboxic trace metal geochemistry in the eastern tropical North Pacific, Geochim. Cosmochim. Acta, 66, 7, 1139–1158, doi:10.1016/S0016-7037(01)00843-2, 2002.

Nelson, D. M., Anderson, R. F., Barber, R. T., Brzezinski, M. A., Buesseler, K. O., Chase, Z., Collier, R. W., Dickson, M. L., François, R., Hiscock, M. R., Honjo, S., Marra, J., Martin, W. R., Sambrotto, R. N., Sayles, F. L., and Sigmon, D. E.:
595 Vertical budgets for organic carbon and biogenic silica in the Pacific sector of the Southern Ocean, 1996–1998, Deep. Res. Part II Top. Stud. Oceanogr., 49, 1645–1674, doi:10.1016/S0967-0645(02)00005-X, 2002.

Oiwane, H., Ikehara, M., Suganuma, Y., Miura, H., Nakamura, Y., Sato, T., Nogi, Y., Yamane, M., and Yokoyama, Y.: Sediment waves on the Conrad Rise, Southern Indian Ocean: Implications for the migration history of the Antarctic Circumpolar Current, Mar. Geol., 348, 27–36, doi:10.1016/j.margeo.2013.10.008, 2014.

600 Oliver, K. I. C., Hoogakker, B. A. A., Crowhurst, S., Henderson, G. M., Rickaby, R. E. M., Edwards, N. R., and Elderfield, H.: A synthesis of marine sediment core δ^{13}C data over the last 150 000 years, Clim. Past, 6, 645–673, doi:10.5194/cp-6-645-2010, 2010.

Orsi, H., Whitworth, T., and Nowlin Jr, W. D.: On the meridional extent and fronts of the Antarctic Circumpolar Current, Deep. Res. Part I, 42, 5, 641–673, doi:10.1016/0967-0637(95)00021-W, 1995.

605 Pichat, S., Sims, K. W. W., François, R., McManus, J. F., Leger, S. B., and Albarède, F.: Lower export production during glacial periods in the equatorial Pacific derived from $(^{231}Pa/^{230}Th)_{xs,0}$ measurements in deep-sea sediments, Paleoceanography, 19, PA4023, 1–21, doi:10.1029/2003PA000994, 2004.

Pichevin, L. E., Ganeshram, R. S., Geibert, W., Thunell, R., and Hinton, R.: Silica burial enhanced by iron limitation in oceanic upwelling margins, Nat. Geosci., 7, 541–546, doi:10.1038/ngeo2181, 2014.

610 Pollard, R. T., Venables, H. J., Read, J. F., and Allen, J. T.: Large-scale circulation around the Crozet Plateau controls an annual phytoplankton bloom in the Crozet Basin, Deep. Res. Part II Top. Stud. Oceanogr., 54, 1915–1929, doi:10.1016/j.dsr2.2007.06.012, 2007.

Pondaven, P., Ragueneau, O., Tréguer, P., Hauvespre, A., Dezileau, L., Reyss, J. L.: Resolving the 'opal paradox' in the Southern Ocean, Nature, 405, 168–172, doi:10.1038/35012046, 2000.

615 Rae, J. W. B., Burke, A., Robinson, L., Adkins, J. F., Chen, T., Cole, C., Greenop, R., Li, T., Littley, E. F. M., Nita, D. C., Steward, J. A., and Taylor, B. J.: CO_2 storage and release in the deep Southern Ocean on millennial to centennial timescales, Nature, 562, 569–573, doi:10.1038/s41586-018-0614-0, 2018.

Ragueneau, O., Tréguer, P., Leynaert, A., Anderson, R. F., Brzezinski, M. A., DeMaster, D. J., Dugdale, R. C., Dymond, J., Fischer, G., François, R., Heinze, C., Maier-Reimer, E., Martin-Jézéquel, V., Nelson, D. M., and Quéguiner, B.: A review of 620 the Si cycle in the modern ocean: Recent progress and missing gaps in the application of biogenic opal as a paleoproductivity proxy, Glob. Planet. Change, 26, 317–365, doi:10.1016/S0921-8181(00)00052-7, 2000.

Ronge, T. A., Prange, M., Mollenhauer, G., Ellinghausen, M., Kuhn, G., and Tiedemann, R.: Radiocarbon Evidence for the Contribution of the Southern Indian Ocean to the Evolution of Atmospheric CO_2 Over the Last 32,000 Years, Paleoceanogr. Paleoclimatology, 35, doi: 10.1029/2019PA003733, 2020.

625 Sakamoto, T., Kuroki, K., Sugawara, T., Aoike, K., Iijima, K., and Sugisaki, S.: Nondestructive X-ray fluorescence (XRF) core-imaging scanner, TATSCAN-F2, Scientific Drilling, 2, 37–39, 2006.

Sarnthein, M., Schneider, B., and Grootes, P. M.: Peak glacial ^{14}C ventilation ages suggest major draw-down of carbon into the abyssal ocean, Clim. Past, 9, 2595–9614, doi:10.5194/cp-9-2595-2013, 2013.

Sayles, F. L., Martin, W. R., Chase, Z., and Anderson, R. F.: Benthic remineralization and burial of biogenic SiO_2, $CaCO_3$, 630 organic carbon, and detrital material in the Southern Ocean along a transect at 170° West, Deep. Res. Part II Top. Stud. Oceanogr., 48, 19–20, 4323–4383, doi:10.1016/S0967-0645(01)00091-1, 2001.

Schlitzer, R.: Ocean Data View, available at http://odv.awi.de, 2018.

Sigman, D. M. and Boyle, E. A.: Glacial/interglacial variations in atmospheric carbon dioxide, Nature, 407, 859–869, doi:10.1038/35038000, 2000.

635 Sigman, D. M., Hain, M. P., and Haug, G. H.: The polar ocean and glacial cycles in atmospheric CO_2 concentration, Nature, 466, 7302, 47–55, doi:10.1038/nature09149, 2010.

Sigman, D. M., Fripiat, F., Studer , A. S., Kemeny, P. C., Martínez-García, A., Hain, M. P., Ai, X., Wang, X., Ren, H., and Haug, G. H.: The Southern Ocean during the ice ages: A review of the Antarctic surface isolation hypothesis, with comparison to the North Pacific, Quat. Sci. Rev., 254, 106732, doi:10.1016/j.quascirev.2020.106732, 2021.

640 Skinner, L. C.: Glacial-interglacial atmospheric CO_2 change: a possible "standing volume" effect on deep-ocean carbon sequestration, Clim. Past, 5, 537–550, doi:10.5194/cp-5-537-2009, 2009.

Skinner, L. C., Fallon, S., Waelbroeck, C., Michel, E., and Barker, S.: Ventilation of the Deep Southern Ocean and Deglacial CO_2 Rise, Science, 328, 5982, 1147–1151, doi:10.1126/science.1183627, 2010.

Skinner, L. C., Primeau, F., Freeman, E., de la Fuente, M., Goodwin, P. A., Gottschalk, J., Huang, E., McCave, I. N., Noble,

645 T. L., and Scrivner, A. E.: Radiocarbon constraints on the glacial ocean circulation and its impact on atmospheric CO_2, Nat. Commun., 8, 16010, doi:10.1038/ncomms16010, 2017.

Stein, K., Timmermann, A., Young Kwon, E., and Friedrich, T.: Timing and magnitude of Southern Ocean sea ice/carbon cycle feedbacks, Proc. Nat. Acad. Sci., 117, 9, doi:10.1073/pnas.1908670117, 2020.

Studer, A. S., Sigman, D. M., Martínez-García, A., Benz, V., Winckler, G., Kuhn, G., Esper, O., Lamy, F., Jaccard, S. L.,

650 Wacker, L., Oleynik, S., Gersonde, R., and Haug, G. H.: Antarctic Zone nutrient conditions during the last two glacial cycles, Paleoceanography, 30, 845–862, doi:10.1002/2014PA002745, 2015.

Talley, L. D.: Closure of the global overturning circulation through the Indian, Pacific, and Southern Oceans: Schematics and transports, Oceanography, 26, 80–97, doi:10.5670/oceanog.2013.07, 2013.

Thöle, L. M., Amsler, H. E., Moretti, S., Auderset, A., Gilgannon, J., Lippold, J., Vogel, H., Crosta, X., Mazaud, A., Michel,

655 E., Martínez-García, A., and Jaccard, S. L.: Glacial-interglacial dust and export production records from the Southern Indian Ocean, Earth Planet. Sci. Lett., 525, doi:10.1016/j.epsl.2019.115716, 2019.

Thomson, J., Wallace, H. E., Colley, S., and Toole, J.: Authigenic uranium in Atlantic sediments of the last glacial stage – a diagenetic phenomenon, Earth Planet. Sci. Lett., 98, 222–232, doi:10.1016/0012-821x(90)90061-2, 1990.

Toggweiler, J. R.: Variation of atmospheric CO_2 by ventilation of the ocean's deepest water, Paleoceanography, 14, 5, 571–

660 588, doi:10.1029/1999PA900033, 1999.

Toggweiler, J. R., Russell, J. L., and Carson, S. R.: Midlatitude westerlies, atmospheric CO_2, and climate change during the ice ages, Paleoceanography, 21, PA2005, doi:10.1029/2005PA001154, 2006.

Tribovillard, N., Algeo, T. J., Lyons, T., and Riboulleau, A.: Trace metals as paleoredox and paleoproductivity proxies: An update, Chem. Geol., 232, 1–2, 12–32, doi:10.1016/j.chemgeo.2006.02.012, 2006.

665 Vogel, H., Meyer-Jacob, C., Thöle, L. M., Lippold, J. A., Jaccard, S. L.: Quantification of biogenic silica by means of Fourier transform infrared spectroscopy (FTIRS) in marine sediments, Limnol. Oceanogr. Methods, 14, 828–838, doi:10.1002/lom3.10129, 2016.

Watson, A. J. and Naveira Garabato, A. C.: The role of Southern Ocean mixing and upwelling in glacial-interglacial atmospheric CO_2 change, Tellus, Ser. B Chem. Phys. Meteorol., 58, 1, 73–87, doi:10.1111/j.1600-0889.2005.00167.x, 2006.

670   Watson, A. J., Vallis, G. K., and Nikurashin, M.: Southern Ocean buoyancy forcing of ocean ventilation and glacial
       atmospheric CO_2, Nat. Geosci., 8, 11, 861–864, doi:10.1038/ngeo2538, 2015.

       Wilson, D. J., Piotrowski, A. M., Galy, A., and Banakar, V. K.: Interhemispheric controls on deep ocean circulation and
       carbon chemistry during the last two glacial cycles, Paleoceanography, 30, 621–641, doi:10.1002/2014PA002707, 2015.

       Wolff, E. W., Barbante, C., Becagli, S., Bigler, M., Boutron, C. F., Castellano, E., de Angelis, M., Federer, U., Fischer, H.,
675   Fundel, F., Hansson, M., Hutterli, M., Jonsell, U., Karlin, T., Kaufmann, P., Lambert, F., Littot, G. C., Mulvaney, R.,
       Röthlisberger, R., Ruth, U., Severi, M., Siggaard-Andersen, M. L., Sime, L. C., Steffensen, J. P., Stocker, T. F., Traversi, R.,
       Twarloh, B., Udisti, R., Wagenbach, D., and Wegner, A.: Changes in environment over the last 800,000 years from chemical
       analysis of the EPICA Dome C ice core, Quat. Sci. Rev., 29, 285–295, doi:10.1016/j.quascirev.2009.06.013, 2010.

       Xiao, W., Esper, O., and Gersonde, R.: Last Glacial - Holocene climate variability in the Atlantic sector of the Southern
680   Ocean. Quat. Sci. Rev. 135, 115–137. doi: 10.1016/j.quascirev.2016.01.023, 2016.

       Yu, J., Menviel, L., Jin, Z. D., Thornalley, D. J. R., Barker, S., Marino, G., Rohling, E. J., Cai, Y., Zhang, F., Wang, X., Dai,
       Y., Chen, P., and Broecker, W. S.: Sequestration of carbon in the deep Atlantic during the last glaciation, Nat. Geosci., 9,
       319–324, doi:10.1038/ngeo2657, 2016.

       Zielinski, U. and Gersonde, R.: Plio-Pleistocene diatom biostratigraphy from ODP Leg 177, Atlantic sector of the Southern
685   Ocean, Mar. Micropaleontol., 45, 225–268, doi:10.1016/S0377-8398(02)00031-2, 2002.
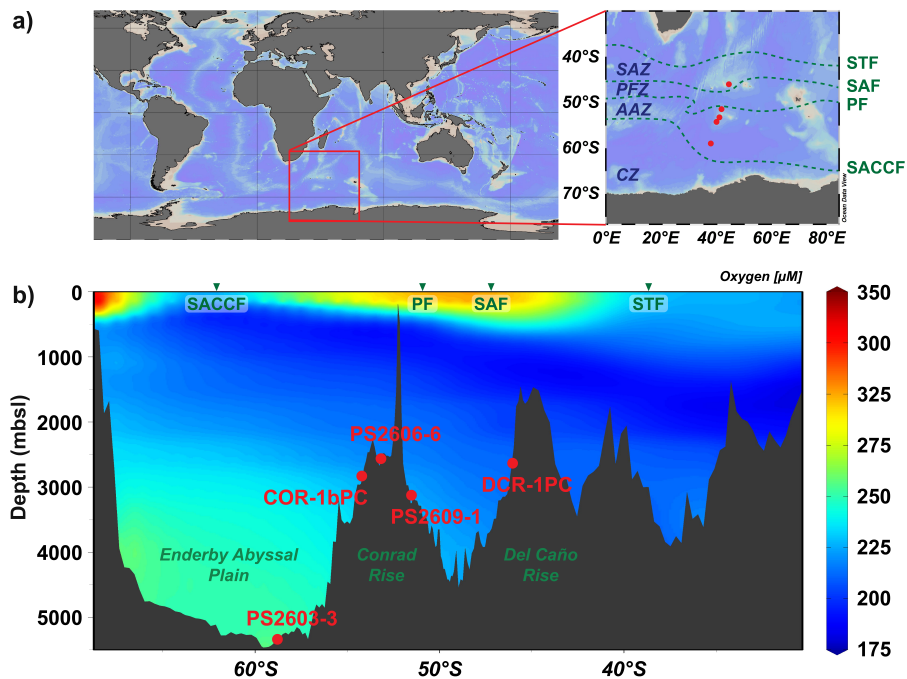
Figure 1: a) Core locations in the SW Indian Ocean across the Southern Ocean frontal system. The fronts from north to south are the Subtropical Front (STF), Subantarctic Front (SAF), Polar Front (PF), and the Southern ACC Front (SACCF); the zones between them are defined as the Subantarctic Zone (SAZ), Polar Frontal Zone (PFZ), Antarctic Zone (AZ), and Continental Zone (CZ) (Orsi et al., 1995). b) Cross section of core locations with modern oxygen concentrations (plotted with the ODV-software, Schlitzer, 2018).

690
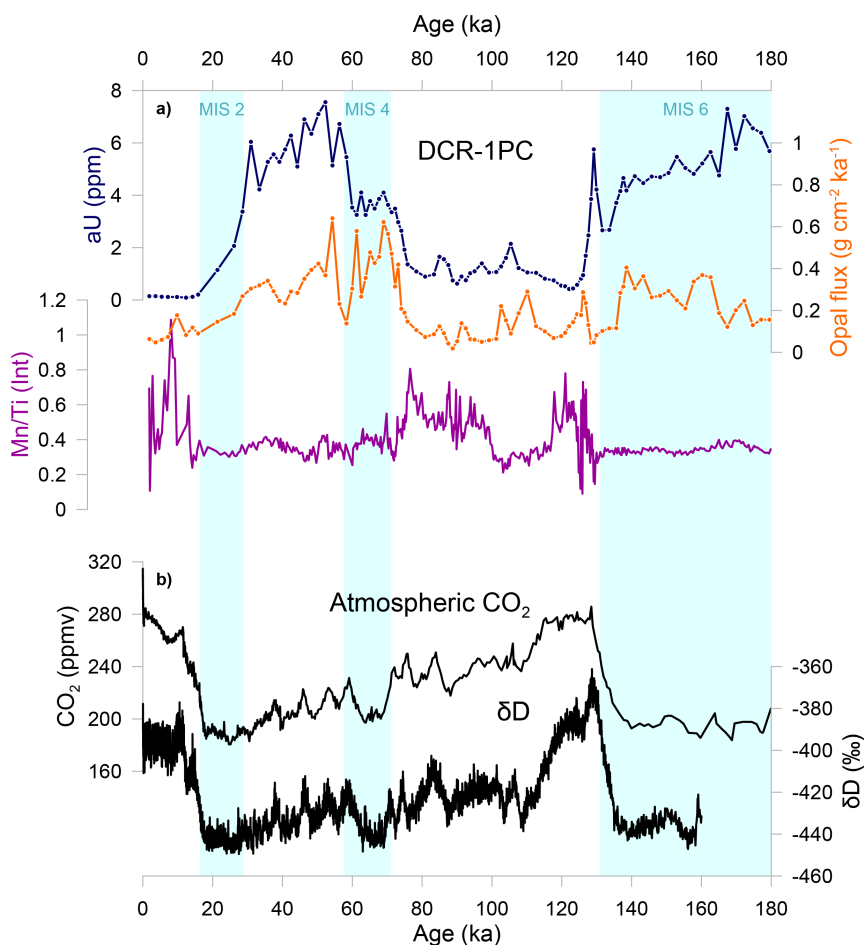
695 **Figure 2: a) Authigenic uranium concentrations (in blue), opal fluxes (in orange) and Mn/Ti ratios (in purple) from XRF-scanning in the Subantarctic Zone. b) Atmospheric CO$_2$ concentrations from EPICA Dome C ice core, composite record (Bereiter et al., 2015 *and references therein*) and δD record from EPICA Dome C ice core reflecting Antarctic air temperatures (Jouzel et al., 2007). Light blue bars show cold periods MIS 2, 4, and 6 (Lisiecki and Raymo, 2005).**
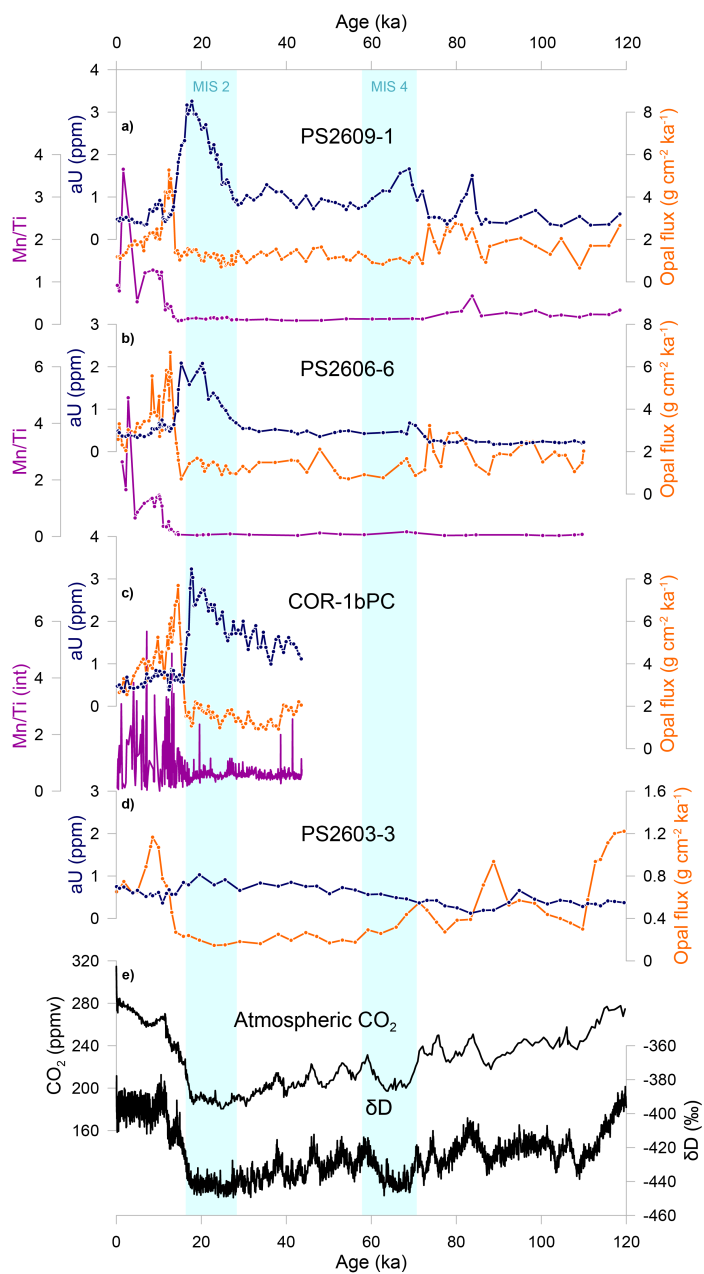
Figure 3: a)–d) Authigenic uranium concentrations (in blue), opal fluxes (in orange), and Mn/Ti ratios (in purple) in the Antarctic Zone south of the Polar Front. e) Atmospheric CO₂ from EPICA Dome C ice core, composite record (Bereiter et al., 2015 *and references therein*) and δD record from EPICA Dome C ice core reflecting Antarctic air temperatures (Jouzel et al., 2007). Light blue bars show cold periods MIS 2 and 4 (Lisiecki and Raymo, 2005).

705
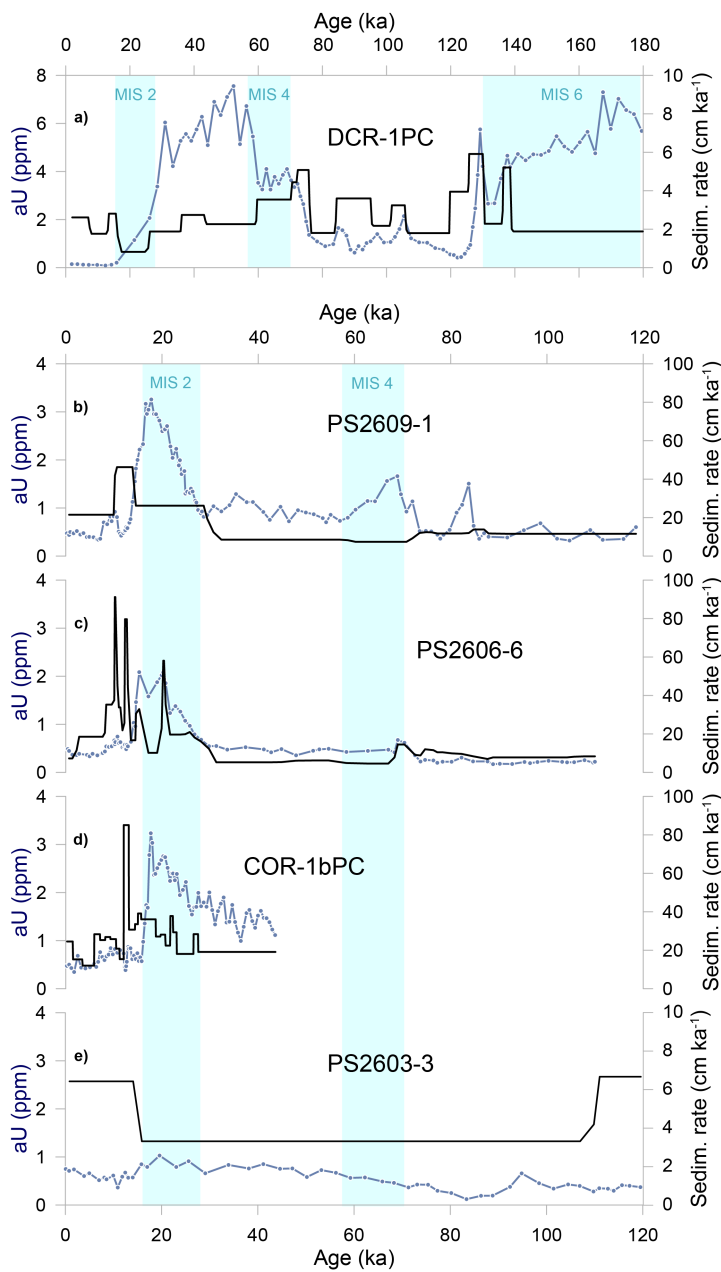
Figure 4: a)–e) Sedimentation rates (in black) and authigenic uranium concentrations (in light blue) in all cores from north to south. Light blue bars show cold periods MIS 2, 4, and 6 (Lisiecki and Raymo, 2005).

710

715

720

725

730

735

Table 1: Tie points of cores PS2609-1, PS2606-6, and PS2603-3. MagSus = magnetic susceptibility; BSiO$_2$ = biogenic silica; LR04 = global benthic δ^{18}O LR04-stack (Lisiecki and Raymo, 2005); EDC = Epica Dome C (Lambert et al., 2012).

Tie points PS2609-1

Depth (cm)	Age pointers (ka)	based on
0	0	
215	10	Ca peak
400	14	MagSus vs LR04; BSiO$_2$ vs LR04; Si/Ti vs LR04
785	28.68	Ti (XRF) vs EDC dust
808	29.88	Ti (XRF) vs EDC dust
1050	58.2	Ti (XRF) vs EDC dust
1145	71	MagSus vs LR04; Fe vs LR04
1157	72.25	Ti (XRF) vs EDC dust
1202	75.87	Ti (XRF) vs EDC dust
1293	83.6	Ti (XRF) vs EDC dust
1340	87	MagSus vs LR04; Fe vs LR04
1595	109	MagSus vs LR04; Fe vs LR04

Tie points PS2603-3

Depth (cm)	Age pointers (ka)	based on
0	0	
90	14	BSiO$_2$ vs LR04; rouxia lenenterae
405	109	BSiO$_2$ vs LR04; hemidiscus karstenii
545	130	BSiO$_2$ vs LR04
640	191	BSiO$_2$ vs LR04; rouxia constricta
690	243	BSiO$_2$ vs LR04
910	300	BSiO$_2$ vs LR04

Tie points PS2606-6

Depth (cm)	Age pointers (ka)	based on
0	0	
14	1.92	14C - Xiao et al. (2016)
128	8.08	14C - Xiao et al. (2016)
198	10.06	14C - Xiao et al. (2016)
228	10.39	14C - Xiao et al. (2016)
266	11.51	Ca/Ti (XRF) vs EPICA dome C dust
275	12.12	14C - Xiao et al. (2016)
328	12.79	Ca/Ti (XRF) vs EPICA dome C dust
357	14.52	14C - Xiao et al. (2016)
380	15.07	Ca/Ti (XRF) vs EPICA dome C dust
427	19.68	14C - Xiao et al. (2016)
478	20.56	Ti (XRF) vs EDC dust
559	24.67	Ti (XRF) vs EDC dust
591	26.20	Ti (XRF) vs EDC dust
639	29.20	Ti (XRF) vs EDC dust
719	44.39	Ti (XRF) vs EDC dust
725	45.44	Ti (XRF) vs EDC dust
786	55.27	Ti (XRF) vs EDC dust
844	67.90	MagSus vs LR04; Ti, Ca (XRF) vs EDC dust
889	71	MagSus vs LR04
905	73.30	Ca/Ti (XRF) vs EDC dust
936	75.87	Ti (XRF) vs EDC dust
968	78.93	Ca/Ti (XRF) vs EDC dust
1013	83.6	Ca/Ti (XRF) vs EDC dust
1036	87	MagSus vs LR04; Ti, Ca (XRF) vs EDC dust
1174	104.69	Ca/Ti (XRF) vs EDC dust
1210	109	MagSus vs LR04